Available online at www.sciencedirect.com
SCIENCE DIRECT
Journal of Sound and Vibration 295 (2006) 76–93
JOURNAL OF SOUND AND VIBRATION
www.elsevier.com/locate/jsvi

Eigenvalue analysis of doubly connected plates with different configurations

Anand V. Singh*, Muhammad Tanveer

Department of Mechanical and Materials Engineering, The University of Western Ontario, London, Ontario, Canada N6A 5B9

Received 12 May 2005; received in revised form 28 November 2005; accepted 16 December 2005
Available online 10 March 2006

Abstract

This paper deals with the vibration and buckling analyses of the first-order shear deformable rhombic and square plates using a p-type variational method. The formulation includes rotary inertia and transverse shear terms. The full plate is modeled with a single domain defined by a set of geometric points in the plane of the plate. Square and rectangular plates with a circular hole at the center are treated as the numerical example for the doubly connected plate and are modeled using one quarter of the geometry and only two elements. The symmetry about x and y axes with regards to load and boundary conditions are exploited. Buckling coefficients and natural frequencies are calculated and compared with results from the published sources and the finite element method.

1. Introduction

Thin plate with an opening can be found in the form of many practical load-bearing structural components in aerospace and ship building industries. Literally, thousands of research papers have been published in the literature over the last several decades on the buckling and vibration of plates. In this paper, only a few studies by others with direct relevance are briefly discussed in the following. The plate buckling problem has been studied using both the analytical and numerical methods (Timoshenko and Gere [1], and Bulson [2]). Leissa and Kang [3,4] presented an exact solution procedure for the buckling analysis of rectangular plates having two opposite edges simply supported (SSSS) as well as subjected to linearly varying in-plane normal stress. They have enlisted some of the earlier useful works on this subject. Dickinson and co-workers [5–7] used Rayleigh–Ritz method for the vibration and buckling analyses of rectangular plates. Around and during the 1980s, Mizusawa and co-workers published a series of papers which can be cited in their paper [8,9] on the buckling and vibration of skew plates. Liew et al. [10] published a review paper on the vibration of first-order shear deformable plate citing 132 publications. Then Liew and co-workers [11–18] published a series of papers on the bending, buckling and vibration of different shaped plates. Buckling of rectangular plates with eccentric holes has also been studied and reported in the literature (El-Sawy and Nazmy [19]). Similarly, through a simple literature search, one can find published works on the vibration of various shaped plates with cutouts

*Corresponding author. Tel.: +1 519 661 2111; fax: +1 519 661 3030.
E-mail address: avsingh@eng.uwo.ca (A.V. Singh).

0022-460X/$ - see front matter © 2006 Elsevier Ltd. All rights reserved.
doi:10.1016/j.jsv.2005.12.044

like the one by Huang and Sakiyama [20]. The authors of this paper also published their work on the vibration, bending and buckling of various shaped plates [21–23], wherein they used a modified form of the Ritz method.

This paper presents the vibration and buckling analyses using a displacement based p-type numerical method of first-order shear deformable rhombic and square plates with and without openings. This method permits analysis of a plate without the hole by considering the model represented by only one quadrilateral domain and the accuracy in the results can be improved by increasing the order of the polynomials used for the displacement fields. Similarly, the analysis of a doubly connected plate problems has been performed with only two sub-regions in the quarter section of the geometry and the use of symmetry conditions with regards to geometry, boundary and loading has been made. The convergence studies are also performed in this paper for the buckling of rhombic plate and square plate with a circular hole at the center. Numerical results in dimensionless form corresponding to buckling coefficient ($k = P_{cr}a/\pi^2 D$) and frequency parameter $\left(\lambda = \omega a^2\sqrt{\rho h/D}\right)$ in terms of the load, length, thickness, mass density and flexural rigidity are calculated and compared with the published results in Refs. [11,14,16] and also with the finite element method using I-DEAS [25]. Variations of the buckling coefficient (k) and frequency parameter (λ) with the plate thickness and the hole diameter are also presented graphically and discussed in this paper.

2. Equations for the elastic plate

The displacement components (u', v', w') along the Cartesian axes (x, y, z), respectively, at an arbitrary point in the plate are expressed in matrix form as

$$\{\hat{u}\} = [Z_1]\{\Delta\}, \tag{1}$$

where

$$\{\hat{u}\}^{\mathrm{T}} = \{\, u' \quad v' \quad w' \,\}, \quad \{\Delta\}^{\mathrm{T}} = \{\, u \quad v \quad w \quad \beta_1 \quad \beta_2 \,\}, \quad [Z_1] = \begin{bmatrix} 1 & 0 & 0 & z & 0 \\ 0 & 1 & 0 & 0 & z \\ 0 & 0 & 1 & 0 & 0 \end{bmatrix}.$$

Also, (u, v, w) denote the displacement components at the middle plane of the plate in (x, y, z) directions, respectively, and (β_1, β_2) are the components of rotation of the normal to the middle plane. Coordinate z is measured along the perpendicular to the middle plane.

The strain–displacement relationship is derived as

$$\{\varepsilon'\} = [Z]\{X\} \quad \text{and} \quad \{X\} = [d]\{\Delta\}, \tag{2}$$

where

$$\{\varepsilon'\}^{\mathrm{T}} = \{\, \varepsilon'_x \quad \varepsilon'_y \quad \gamma'_{xy} \quad \gamma'_{yz} \quad \gamma'_{zx} \,\},$$

$$\{X\}^{\mathrm{T}} = \{\, \varepsilon_x \quad \varepsilon_y \quad \gamma_{xy} \quad \gamma_{yz} \quad \gamma_{zx} \quad a\kappa_x \quad a\kappa_y \quad a\kappa_{xy} \,\},$$

$$\varepsilon_x = \frac{\partial u}{\partial x}, \quad \varepsilon_y = \frac{\partial v}{\partial y}, \quad \gamma_{xy} = \frac{\partial u}{\partial y} + \frac{\partial v}{\partial x}, \quad \gamma_{yz} = \frac{\partial w}{\partial y} + \beta_2, \quad \gamma_{zx} = \frac{\partial w}{\partial x} + \beta_1,$$
$$ak_x = \frac{\partial \beta_1}{\partial x}, \quad ak_y = \frac{\partial \beta_2}{\partial y}, \quad ak_{xy} = \frac{\partial \beta_1}{\partial y} + \frac{\partial \beta_2}{\partial x}. \tag{3}$$

$$[Z] = \begin{bmatrix} 1 & 0 & 0 & 0 & 0 & z & 0 & 0 \\ 0 & 1 & 0 & 0 & 0 & 0 & z & 0 \\ 0 & 0 & 1 & 0 & 0 & 0 & 0 & z \\ 0 & 0 & 0 & 1 & 0 & 0 & 0 & 0 \\ 0 & 0 & 0 & 0 & 1 & 0 & 0 & 0 \end{bmatrix},$$

$$[d]^{\mathrm{T}} = \begin{bmatrix} \frac{\partial}{\partial x} & 0 & \frac{\partial}{\partial y} & 0 & 0 & 0 & 0 & 0 \\ 0 & \frac{\partial}{\partial y} & \frac{\partial}{\partial x} & 0 & 0 & 0 & 0 & 0 \\ 0 & 0 & \frac{\partial}{\partial y} & \frac{\partial}{\partial x} & 0 & 0 & 0 & 0 \\ 0 & 0 & 0 & 0 & 1 & \frac{\partial}{\partial x} & 0 & \frac{\partial}{\partial y} \\ 0 & 0 & 0 & 1 & 0 & 0 & \frac{\partial}{\partial y} & \frac{\partial}{\partial x} \end{bmatrix}.$$

The strain energy is given by

$$\mathrm{d}U = \tfrac{1}{2}\{\varepsilon'\}^{\mathrm{T}}[E]\{\varepsilon'\}\,\mathrm{d}x\,\mathrm{d}y\,\mathrm{d}z = \tfrac{1}{2}\{X\}^{\mathrm{T}}([Z]^{\mathrm{T}}[E][Z]\,\mathrm{d}z)\{X\}\,\mathrm{d}x\,\mathrm{d}y, \tag{4}$$

where matrix $[E]$ is of fifth order and composed of the elastic modulus (E), the Poisson's ratio (v) and $k_{\mathrm{scf}} = 5/6$ is the shear correction factor used here to compensate for the parabolic distribution of the transverse shear stress. The non-zero terms of $[E]$ are as follows:

$$\begin{aligned} &E_{11} = E_{22} = E/(1-v^2),\ \ E_{12} = E_{21} = vE_{11},\ \ E_{33} = (1/2)E/(1+v), \\ &E_{44} = E_{55} = k_{\mathrm{scf}}E_{33}. \end{aligned} \tag{5}$$

In a similar manner, the kinetic energy expression can be written as

$$\mathrm{d}K = \tfrac{1}{2}\rho\{\dot{\varepsilon}'\}^{\mathrm{T}}[E]\{\dot{\varepsilon}'\}\,\mathrm{d}x\,\mathrm{d}y\,\mathrm{d}z = \tfrac{1}{2}\{\dot{\Delta}\}^{\mathrm{T}}(\rho[Z_1]^{\mathrm{T}}[Z_1]\,\mathrm{d}z)\{\dot{\Delta}\}\,\mathrm{d}x\,\mathrm{d}y. \tag{6}$$

Here, ρ = mass density of the plate material and over-dot represents the time derivative. Integration of Eqs. (4) and (6) over the thickness of the plate yields

$$U = \frac{1}{2}\iint_{\mathrm{Area}}\{X\}^{\mathrm{T}}[D]\{X\}\,\mathrm{d}x\,\mathrm{d}y, \quad K = \frac{1}{2}\iint_{\mathrm{Area}}\{\dot{\Delta}\}^{\mathrm{T}}[A_0]\{\dot{\Delta}\}\,\mathrm{d}x\,\mathrm{d}y, \tag{7}$$

where matrices $[D]_{8\times 8}$ and $[A_0]_{5\times 5}$ are composed of the geometric and elastic properties of the plate and are given by the integrals

$$[D] = \int_{-h/2}^{+h/2}[Z]^{\mathrm{T}}[E][Z]\,\mathrm{d}z, \quad [A_0] = \rho\int_{-h/2}^{+h/2}[Z_1]^{\mathrm{T}}[Z_1]\,\mathrm{d}z. \tag{8}$$

The non-zero terms in $[D]_{8\times 8}$ are

$$\begin{aligned} &D_{11} = D_{22} = K_0, \quad D_{12} = D_{21} = vK_0, \quad D_{33} = [(1-v)/2]K_0, \quad D_{44} = D_{55} = k_{\mathrm{scf}}K_0, \\ &D_{66} = D_{77} = D_0, \quad D_{67} = D_{76} = vD_0, \quad D_{88} = [(1-v)/2]D_0, \end{aligned} \tag{9}$$

where $K_0 = Eh/(1-v^2)$ and $D_0 = Eh^3/[12(1-v^2)]$ are respectively the extensional and flexural rigidities of the plate. Similarly, matrix $[A_0]_{5\times 5}$ which can be obtained exactly by integrating contains both the translational and rotary inertias. In the above, basic equations for the first-order-shear deformable plate have been presented. In the following section, stiffness matrix, consistent mass matrix and consistent load vector are derived for a defined geometry of the plate.

3. Stiffness and mass matrices for the analysis of a doubly connected plate

Fig. 1 shows the middle plane of an arbitrary-shaped plate with an opening and the annulus is divided into a number of quadrilateral sub-regions. A quadrilateral sub-region is further defined in Fig. 2 by four curved edges and a number of points which can be on and inside the boundary. The thickness (h) of the plate is assumed to be uniform and small in comparison with the other dimensions. The co-ordinates (x, y) of an arbitrary point inside the quadrilateral region, wherein the natural coordinates ξ and η bounded by $-1 \leqslant (\xi, \eta) \leqslant +1$ are defined, can be interpolated using the prescribed coordinates (x_i, y_i) of the geometric points shown in Fig. 2 and the shape function $N_i(\xi, \eta)$ with $i = 1, 2, 3, \ldots, n$ (Weaver

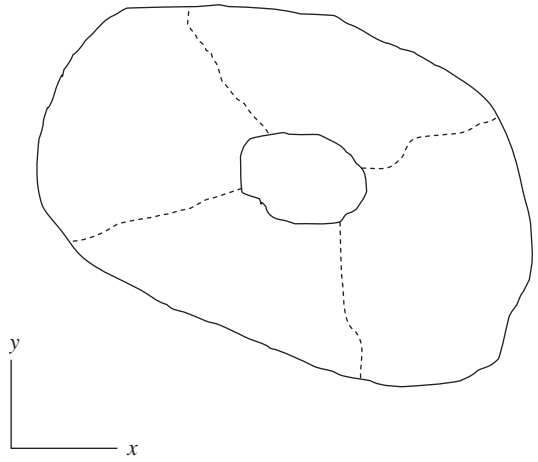

Fig. 1. Middle plane of a doubly connected plate divided into quadrilateral sub-regions.

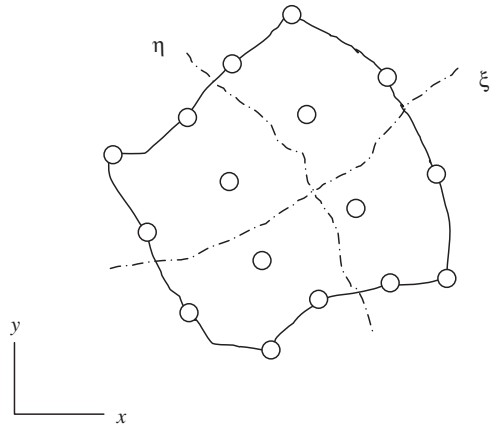

Fig. 2. Natural coordinate system in a quadrilateral domain.

and Johnson [24]):

$$x = \sum_{i=1}^{n} N_i(\xi,\eta)x_i, \quad y = \sum_{i=1}^{n} N_i(\xi,\eta)y_i. \tag{10}$$

In a similar manner, the displacement components can also be interpolated using a different set of preselected points on the quadrilateral domain:

$$u = \sum_{i=1}^{p} f_i(\xi,\eta)U_i, \quad v = \sum_{i=1}^{p} f_i(\xi,\eta)V_i, \quad w = \sum_{i=1}^{p} f_i(\xi,\eta)W_i,$$
$$\beta_1 = \sum_{i=1}^{p} f_i(\xi,\eta)\theta_i, \quad \beta_2 = \sum_{i=1}^{p} f_i(\xi,\eta)\phi_i. \tag{11}$$

In the above equations, $f_i(\xi,\eta)$ is the displacement shape function and indices U_i, V_i, W_i, θ_i and ϕ_i correspond to u, v, w, β_1 and β_2 respectively, at the ith displacement node. In this work, u and v are used only in the buckling load calculations as discussed in Ref. [23]. For the flexure of the plate only, the orders of matrices $[D]$ and $[A_0]$ in Eq. (8) will be fifth and third respectively. If ℓ and m denote the orders of the polynomials in x and

y, respectively, the number of displacement nodes required is $p = (\ell + 1)(m + 1)$. Eq. (11) can be expressed in matrix form as

$$\{\Delta\} = [\bar{F}(\xi, \eta)]\{\Gamma\}, \tag{12}$$

where $\{\Gamma\}^{\mathrm{T}} = \left\{ W_1 \quad \theta_1 \quad \phi_1 \quad W_2 \quad \theta_2 \quad \phi_2 \quad - \quad - \quad - \quad W_n \quad \theta_n \quad \phi_n \right\}$ and $[\bar{F}(\xi, \eta)]_{3\times 3n} = [[F_1(\xi, \eta)] [F_2(\xi, \eta)][F_3(\xi, \eta)] - - [F_n(\xi, \eta)]]$. Matrix $[F_i(\xi, \eta)]_{3x3}$ in which $i = 1, 2, 3, \ldots n$, is given as

$$[F(x, y)] = \begin{bmatrix} f_i(\xi, \eta) & 0 & 0 \\ 0 & f_i(\xi, \eta) & 0 \\ 0 & 0 & f_i(\xi, \eta) \end{bmatrix}. \tag{13}$$

Using Eq. (12) in Eq. (2), the following is obtained:

$$\{X\} = [d][\bar{F}(\xi, \eta)]\{\Gamma\} = [B]\{\Gamma\}, \tag{14}$$

where $[B]_{5\times 5p} = [d][\bar{F}(\xi, \eta)]$ and is not presented in its detailed form because of large size. Now, by substituting Eq. (14) into Eq. (7), the following can be arrived at

$$U = \tfrac{1}{2}\{\Gamma\}^{\mathrm{T}}[k]\{\Gamma\} \quad \text{and} \quad K = \tfrac{1}{2}\{\dot{\Gamma}\}^{\mathrm{T}}[M]\{\dot{\Gamma}\}. \tag{15}$$

Here, matrix $[k]$ represents the stiffness matrix of the whole plate and is given by

$$[k] = \int_{-1}^{+1}\int_{-1}^{+1} [B]^{\mathrm{T}}[D][B]|J(\xi, \eta)|\,\mathrm{d}\xi\,\mathrm{d}\eta.$$

Similarly, the mass matrix consistent with the prescribed displacement field is given by

$$[M] = \int_{-1}^{+1}\int_{-1}^{+1} [\bar{F}(\xi, \eta)]^{\mathrm{T}}[A_0][\bar{F}(\xi, \eta)]|J(\xi, \eta)|\,\mathrm{d}\xi\,\mathrm{d}\eta. \tag{16}$$

To calculate the stiffness and mass matrices given above in Eq. (16), the integration will be carried out numerically over the entire domain of the plate using the Gauss-method, in which the number of Gauss points to be used will depend upon the orders of the interpolating polynomials that have been used in the geometric and displacement fields (Eqs. (10) and (11)). The stiffness and mass matrices for each quadrilateral region will be assembled to get the same for the doubly connected plate. For the linear plate problems, the in-plane and bending equations are decoupled meaning that the two modes of deformation can be evaluated separately.

4. Buckling analysis

A method to obtain the bucking load is discussed in this section for a plate segment bounded by four edges as shown in Fig. 2. To calculate the buckling load under the membrane stresses σ_x, σ_y and σ_{xy} due to an in-plane load on the plate under investigation, the following equation is used (Bulson [2]):

$$T = \frac{1}{2}\,h \iint_{\text{Area}} \left\{ \frac{\partial w}{\partial x} \quad \frac{\partial w}{\partial y} \right\} \begin{bmatrix} \sigma_x & \sigma_{xy} \\ \sigma_{xy} & \sigma_y \end{bmatrix} \begin{Bmatrix} \dfrac{\partial w}{\partial x} \\ \dfrac{\partial w}{\partial y} \end{Bmatrix} \mathrm{d}x\,\mathrm{d}y. \tag{17}$$

Substituting Eq. (11), which represents the displacement fields, into the above, the following can be deduced after some simple algebra:

$$T = \tfrac{1}{2}\{\Gamma\}^{\mathrm{T}}[K_L]\{\Gamma\}, \tag{18}$$

wherein a vector $\{\Gamma\}$ has been defined in Eq. (12) and $[K_L]$ is the load matrix, which will be obtained via numerical integration using the Gauss method. While integrating for $[K_L]$, the state of in-plane stress at each integration point is secured first from the analysis using only the displacement fields for u and v. Taking the variation of the potential energy, one can easily derive the equilibrium equation $([k] + P_{\mathrm{cr}}[K_L])\{\Gamma\} = 0$, which is an eigenvalue problem. The symbol P_{cr} is the critical in-plane load applied to the edge of the plate. It is a

standard practice to calculate the values of the buckling coefficient $k = P_{cr}a/(\pi^2 D)$ for plate buckling problems. In this paper also, the buckling coefficient has been calculated for rhombic and square plates subject to different boundary and loading conditions.

4.1. Square and rhombic plates

For a full plate without the opening, four corner points are used as the geometric nodes. The orders of the interpolating polynomials in ξ and η of Eq. (11) are taken to be equal, i.e. $\ell = m$, in the numerical calculations. To examine the validity of the method, a convergence study is performed on a rhombic plate with $a = b, h/a = 0.05$ and skew angles of $\alpha = 0^\circ, 15^\circ, 30^\circ, 45^\circ, 60^\circ$ and 75° (as shown in Fig. 3). All four sides of the plate are simply supported (SSSS) and the computation for this purpose begins with the second order polynomial and ends with the 16th order. The numerical values for the buckling coefficient k are plotted in Fig. 5 against the order of polynomials ℓ or m in each of ξ and η, respectively. Convergence is achieved monotonically with all six cases involving skew angle (α) ranging from 0° to 75°. It is found in this figure that using higher than tenth order polynomials in ξ and η yield accurate results for the cases with $\alpha = 0 - 60^\circ$, whereas for skew angle 75° more terms are required in the displacement fields. Also seen in here is that in the case of 15° skew angle, the value of k jumps a little showing that the use of 16th and higher order polynomials in the displacement fields can produce numerical instability. Such instability in the calculation does arise due to the fact that there is a considerable amount of mismatch between the first and last coefficients of the polynomials, if the order of the polynomials in the displacement fields is very high. Again, in some cases, it can be obvious, whereas in others it may not be present. However, sixteenth order polynomials are really very high in this type of calculations. Results calculated using twelfth-order polynomials for square plates from the present method are next compared with those obtained by a commercially available computer code I-DEAS [25] and also with the published data in the literature [16], which are presented in Table 1. An excellent agreement is observed here. Presented in Table 2 are the results for skew plates without a hole from the present method along with the appropriate data published by other researchers [11,14]. Two values of the thickness parameter $h/a = 0.10$ and 0.05; Poisson's ratio $\nu = 0.3$; and skew angles $\alpha = 0^\circ, 15^\circ, 30^\circ, 45^\circ, 60^\circ$ and 75° are considered for the three different combinations, viz. all sides SSSS, all sides clamped (CCCC), and clamped–free–clamped–free (CFCF), respectively. Results in this table are found to be in the neighborhood of 5% of each other. Results for skew angles $\alpha = 60^\circ$ and 75° are included in this table for future references as they are not available elsewhere, to the authors' knowledge.

4.2. Square plate with a circular hole at the center

A square plate with a circular hole at the center and partially and symmetrically loaded over a length of c on the two vertical edges is analyzed using a two element model as shown in Fig. 4 with $a = b$. Each element in the model is defined by a grid of 3×3 geometric points for accurate representation of the plate area. In this case also, the calculation begins with the convergence study by considering the parameters $\nu = 0.3, h/a = 0.01$; the load applied on the entire vertical edge; and three hole sizes with $d/a = 0.1, 0.3$ and 0.5, respectively. From the buckling coefficient (k) versus order of the polynomial plots as shown in Fig. 6, it is found that there is a

Table 1
Buckling coefficient k, for square plate subjected to uniaxial loading on two opposite sides: $h/a = 0.01$, $\nu = 0.3$

c/a	SSSS			CCCC			CFCF		
	P.M.	I-DEAS	Ref. [16]	P.M.	I-DEAS	Ref. [16]	P.M.	I-DEAS	Ref. [16]
0	2.69	2.60	2.60	6.89	6.68	6.86	3.79	3.64	3.68
0.25	2.76	2.71	2.73	7.14	7.05	7.19	3.80	3.70	3.74
0.50	3.05	3.04	3.04	8.06	8.02	8.21	3.88	3.83	3.92
0.75	3.52	3.52	—	8.79	9.08	—	3.95	3.93	—
1.00	4.00	4.00	3.97	10.05	10.05	10.15	3.91	3.91	3.91

Table 2
Buckling coefficient k, for skew plates subjected to uniaxial compressive loading with different boundary conditions ($v = 0.3$)

B.C	h/a	Skew angle (α) (deg)	P.M.	Ref. [14]	Ref. [11]
SSSS	0.1	0	3.79	3.73	3.79
		15	3.94	4.05	4.14
		30	5.11	4.85	4.93
		45	8.00	7.61	7.72
		60	14.90	—	—
		75	32.93	—	—
	0.05	0	3.94	3.93	3.94
		15	4.22	4.33	4.33
		30	5.54	5.39	5.42
		45	8.94	8.69	8.74
		60	18.41	—	—
		75	57.04	—	—
CCCC	0.1	0	8.29	8.18	8.29
		15	8.77	8.76	8.77
		30	10.63	10.33	10.38
		45	13.69	13.29	13.69
		60	20.23	—	—
		75	37.74	—	—
	0.05	0	9.56	9.54	9.56
		15	10.23	10.21	10.23
		30	12.58	12.52	12.57
		45	17.96	17.82	17.97
		60	31.28	—	—
		75	84.39	—	—
CFCF	0.1	0	3.51	3.51	3.51
		15	3.79	3.77	3.79
		30	4.81	4.78	4.80
		45	6.33	6.31	6.33
		60	9.31	—	—
		75	18.81	—	—
	0.05	0	3.80	3.80	3.80
		15	4.14	4.13	4.14
		30	5.36	5.35	5.37
		45	7.46	7.37	7.47
		60	11.90	—	—
		75	29.83	—	—

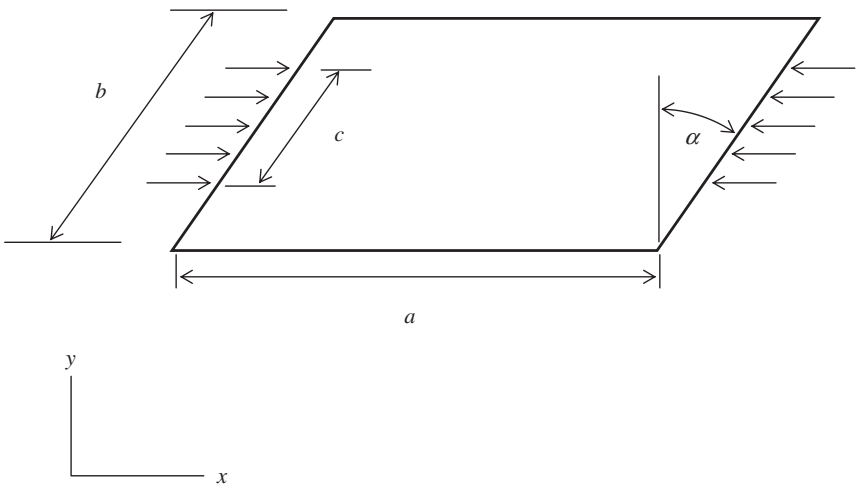

Fig. 3. Skew plate subject to compressive load only on part of the edge.

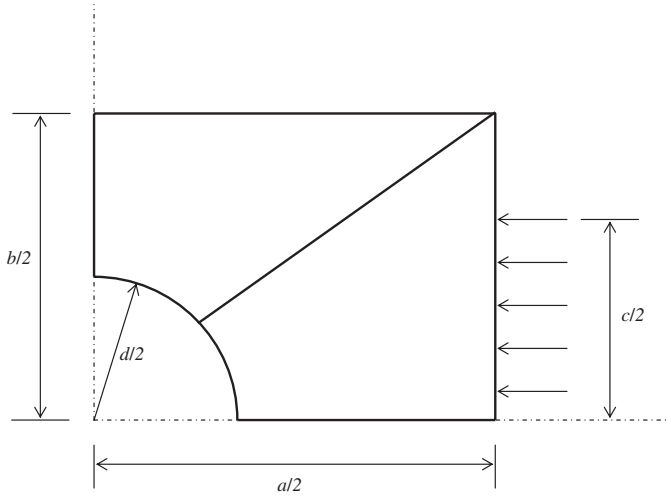

Fig. 4. Quarter model for a rectangular plate subject to partial in-plane edge load with a circular opening at the center.

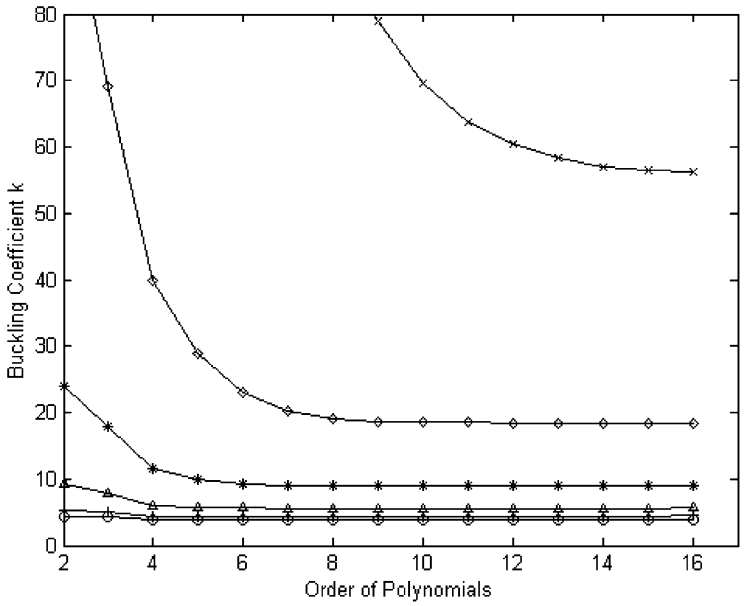

Fig. 5. Buckling coefficient (k) versus order of the polynomials for the convergence study on a simply supported skew plate with $h/a = 0.05$: $\times$, $\alpha = 75°$; $\diamond$, $\alpha = 60°$; $*$, $\alpha = 45°$; $\triangle$, $\alpha = 30°$; $+$, $\alpha = 15°$; $\circ$, $\alpha = 0°$.

rapid convergence in the results. Shown in Fig. 7 are the values of the buckling coefficient from the present method using tenth order polynomials and I-DEAS [25] plotted against the hole size parameter (d/a) for two types of loading on the simply supported (SSSS) plate. The value of $c/a = 1.0$ represents the case in which the load is applied on the full width of the vertical edge, whereas the case with $c/a = 0.5$ correspond to the applied load distributed only half the width of the vertical edge. There is good agreement between the results. Agreement is much better for plates with a small diameter hole at the center. The maximum difference in this comparison is 6.7%. To envision the effects of the hole size on the buckling coefficient, extra results are plotted in Fig. 8 for the SSSS case and Fig. 9 for the CFCF case. Four values of the load distribution parameter $c/a = 1.00$, 0.75, 0.50 and 0.25 are considered for each of the two above mentioned boundary conditions in Figs. 8 and 9, respectively. The buckling coefficient (k) decreases with the increase in the hole diameter and

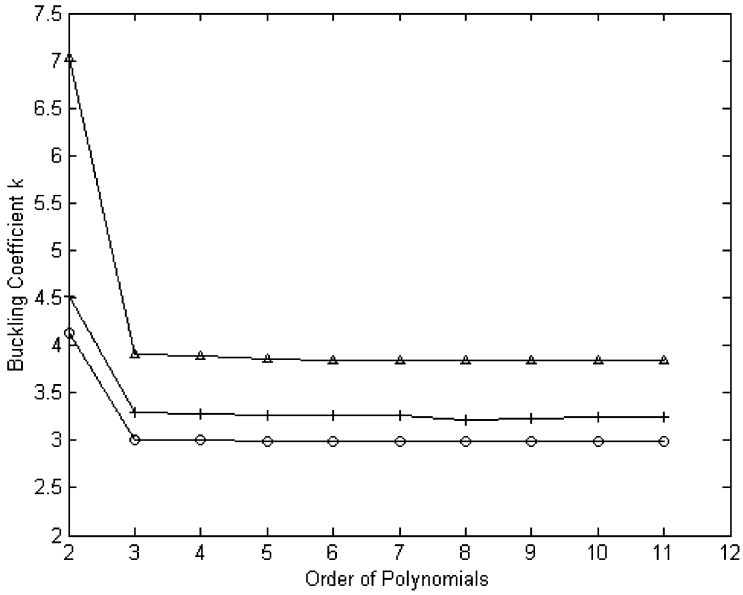

Fig. 6. Buckling coefficient (k) versus order of the polynomials for the convergence study on a simply supported square plate with a circular hole (d/a) at the center. △, $d/a = 0.1$; +, $d/a = 0.3$; ○, $d/a = 0.5$.

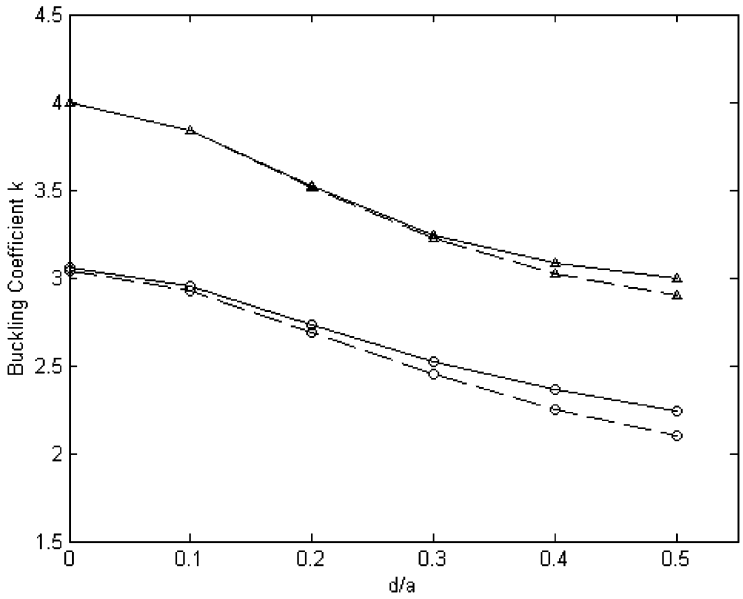

Fig. 7. Buckling coefficient (k) versus the normalized diameter of the hole (d/a) at the center of simply supported square plates with partially loaded edge showing comparison of results from the present method (P.M.) and I-DEAS [25]. Solid line—present method, dashed line—I-DEAS: △, $c/a = 1.0$; ○, $c/a = 0.5$.

also, if the load is spread over the full width of the vertical edges, the stability of the plate is improved. Effects of the plate thickness on the stability of the square plate with a hole ($d/a = 0.25$) at the center can be examined from the results plotted against the thickness parameter (h/a) in Figs. 10 and 11 for the boundary conditions of SSSS and CFCF, respectively. It is noticed that the thickness has very minor influence on the overall stability of the plate. But, the type of distribution of the load represented by parameter (c/a) has significant influence. As higher the value of c/a, the better the stability of the plate.

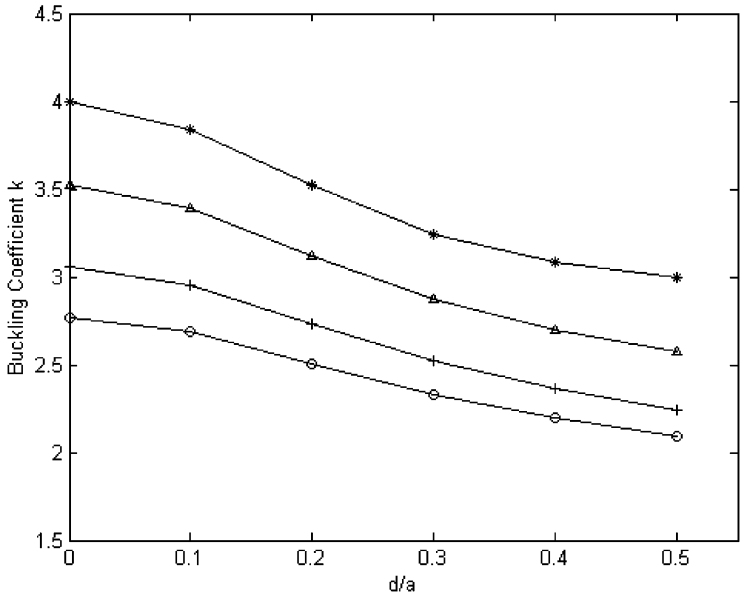

Fig. 8. Buckling coefficient (k) versus the normalized diameter of the hole (d/a) at the center of simply supported square plates with partially loaded edge. $*$, $c/a = 1.0$; $\triangle$, $c/a = 0.75$; $+$, $c/a = 0.5$; $\circ$, $c/a = 0.25$.

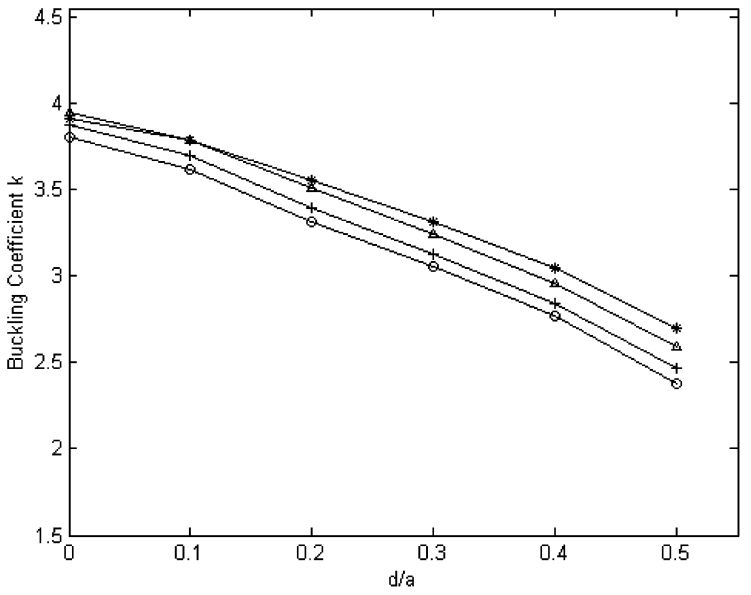

Fig. 9. Buckling coefficient (k) versus the normalized diameter of the hole (d/a) at the center of clamped–free–clamped–free square plates with partially loaded edge. $*$, $c/a = 1.0$; $\triangle$, $c/a = 0.75$; $+$, $c/a = 0.5$; $\circ$, $c/a = 0.25$.

5. Vibration analysis

The matrix equation of motion, $[M]\{\ddot{\Gamma}\} + [k]\{\Gamma\} = 0$, for the free vibration can be derived by the standard procedure of minimization of the potential energy.

In this section, the non-dimensional frequency parameter $\lambda = \omega a^2\sqrt{\rho h/D}$ is calculated first for square and rhombic plates. Using the full plate model and tenth-order polynomials in the displacement field, the first five

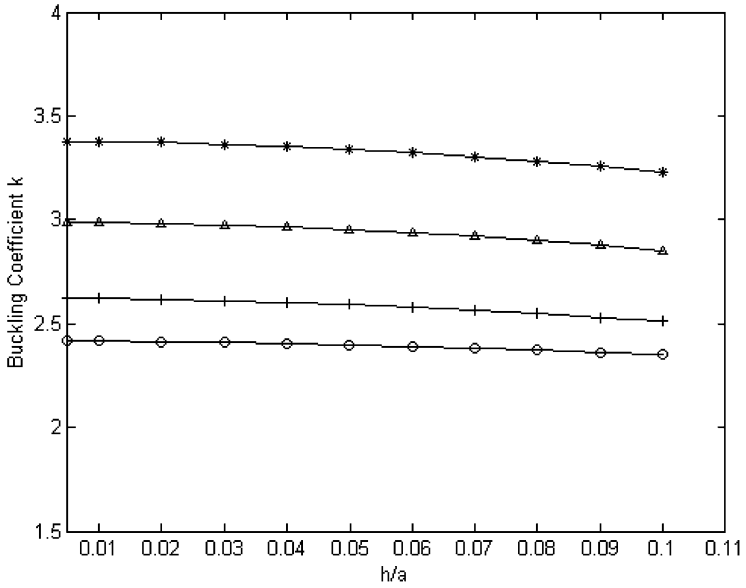

Fig. 10. Buckling coefficient (k) versus normalized thickness (h/a) for simply supported square plate with a circular hole of $d/a = 0.25$ at the center and partially loaded at the edge. $*$, $c/a = 1.0$; $\triangle$, $c/a = 0.75$; $+$, $c/a = 0.5$; $\circ$, $c/a = 0.25$.

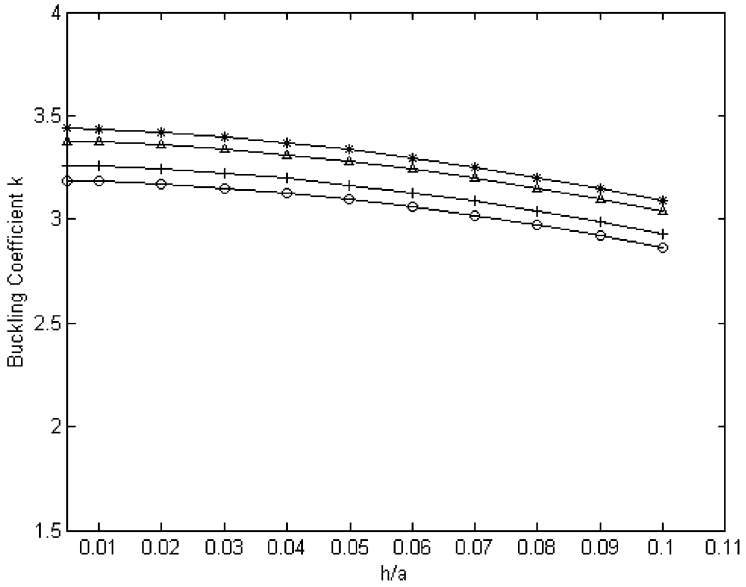

Fig. 11. Buckling coefficient (k) versus normalized thickness (h/a) for clamped–free–clamped–free square plate with a circular hole of $d/a = 0.25$ at the center and partially loaded at the edge. $*$, $c/a = 1.0$; $\triangle$, $c/a = 0.75$; $+$, $c/a = 0.5$; $\circ$, $c/a = 0.25$.

natural frequencies are calculated by the present method and also by I-DEAS for an all side SSSS rhombic plate having a wide range of skew angle, $0 \leqslant \alpha \leqslant 75^\circ$. From the results shown in Table 3, it is found that the two sets of results are in very good agreement. The maximum discrepancy of 4.1% is found in the first frequency for the case with $\alpha = 75^\circ$.

Since the displacement shape functions are attached to the degrees of freedom of each nodal point, it is possible to analyze plates supported at discrete points or only at part of an edge. Therefore, full square and rhombic plates, free along the two horizontal edges and supported only on part of the other two skewed edges,

Table 3
First five dimensionless frequencies $\lambda = \sqrt{\rho h/D}\omega a^2$ for rhombic plates with all sides simply supported ($h/a = 0.01$, $v = 0.3$)

Mode	$\alpha = 0^\circ$		$\alpha = 15^\circ$		$\alpha = 30^\circ$	
	P.M.	I-DEAS	P.M.	I-DEAS	P.M.	I-DEAS
1	19.73	19.73	20.73	20.85	24.69	24.90
2	49.30	49.31	48.11	48.15	52.56	52.58
3	49.30	49.31	55.84	56.04	71.24	71.66
4	78.84	78.86	78.79	78.90	83.39	83.69
5	98.52	98.58	104.43	103.82	122.02	122.52
	$\alpha = 45^\circ$		$\alpha = 60^\circ$		$\alpha = 75^\circ$	
1	34.24	34.90	60.96	63.26	194.57	202.89
2	66.11	66.18	104.51	104.75	280.89	282.24
3	99.54	100.11	146.51	147.58	354.88	359.15
4	106.10	107.26	195.30	195.79	440.53	440.06
5	140.08	140.44	203.60	207.14	539.75	526.53

Table 4
First five dimensionless natural frequencies $\lambda = \sqrt{\rho h/D}\omega a^2$ for square and rhombic plates ($h/a = 0.01, v = 0.3$)

Mode	$c/a = 1.0$		$c/a = 2/3$		$c/a = 1/3$	
	P.M.	I-DEAS	P.M.	I-DEAS	P.M.	I-DEAS
CFCF square plate						
1	22.13	22.14	20.73	19.63	14.47	12.76
2	26.36	26.33	23.21	21.30	15.16	13.85
3	43.31	43.33	40.04	38.01	31.18	29.26
4	61.01	61.04	56.69	51.49	33.63	29.56
5	67.01	66.92	59.39	52.58	34.51	30.05
SFSF square plate						
1	9.62	9.63	9.51	9.45	8.51	8.48
2	16.12	16.09	15.38	14.72	11.43	10.45
3	36.49	36.53	34.36	33.30	26.56	26.35
4	38.88	38.90	38.30	37.28	29.83	26.74
5	46.67	46.61	45.05	42.11	32.07	27.08
SFSF rhombic plate, $\alpha = 30^\circ$						
1	12.10	12.13	11.41	11.31	9.64	9.58
2	17.44	17.61	15.26	15.08	10.97	10.66
3	35.85	35.86	35.33	35.01	27.17	26.11
4	49.08	49.24	43.61	43.25	31.65	28.70
5	60.67	60.89	51.55	49.69	38.71	38.50
CFCF rhombic plate, $\alpha = 30^\circ$						
1	27.319	27.345	24.626	23.013	17.135	15.350
2	30.446	30.437	26.190	24.148	17.987	16.491
3	49.230	49.198	47.450	45.929	35.938	30.531
4	73.532	73.576	64.713	58.867	38.034	32.578
5	80.568	80.414	67.630	60.914	44.953	42.803

are analyzed by the present method and also by the FEM and the results are presented in Table 4. Here, the ratio (c/a) defines the supported portion of an edge, similar to the partially loaded edge shown in Fig. 4. Results from both sources match extremely well for the case of the square plate supported on the full width of the edge for which $c/a = 1.0$. The agreement is not so good for the cases with ($c/a = 2/3$) and ($c/a = 1/3$) and

Table 5
First five dimensionless natural frequencies $\lambda = \sqrt{\rho h/D}\omega a^2$ for square and rectangular plates with a circular hole at the center

Mode	CCCC		CFCF		SFSF	
	P.M.	I-DEAS	P.M.	I-DEAS	P.M.	I-DEAS
Square plate with $a/b = 1.0, h/b = 0.01, d/b = 0.25, v = 0.3$						
1	37.52	37.41	22.39	22.39	9.29	9.29
2	125.22	125.25	43.34	43.30	35.67	35.66
3	145.77	144.97	118.56	118.61	87.58	87.58
4	230.77	230.33	137.48	137.29	122.37	122.43
5	290.11	289.89	159.48	158.70	140.72	139.93
Rectangular plate with $a/b = 2.0, h/b = 0.01, d/b = 0.25, v = 0.3$						
1	99.55	99.22	22.02	22.02	9.32	9.32
2	180.39	179.83	104.43	103.93	86.17	86.09
3	351.38	349.99	118.07	117.94	100.67	100.17
4	492.48	491.36	228.28	226.90	206.28	205.23
5	568.52	568.63	294.73	294.28	242.91	242.41

Table 6
First five dimensionless natural frequencies $\lambda = \sqrt{\rho h/D}\omega a^2$ for square and rectangular plates simply supported on all edges with a circular hole at the center ($h/b = 0.01, v = 0.3$)

Mode	P.M.	I-DEAS	P.M.	I-DEAS	P.M.	I-DEAS
	Square plate					
	$d/b = 0$		$d/b = 0.1$		$d/b = 0.2$	
1	19.73	19.73	19.53	19.49	19.28	19.24
2	98.52	98.56	97.63	97.20	95.83	95.86
3	98.52	98.56	97.71	97.76	101.57	101.06
4	177.07	177.20	176.88	176.54	181.52	181.19
5	255.41	255.67	255.07	253.14	246.83	246.99
	$d/b = 0.3$		$d/b = 0.4$		$d/b = 0.5$	
1	19.48	19.44	20.43	20.39	22.43	22.40
2	93.13	93.15	89.55	89.55	86.47	86.50
3	113.00	112.52	129.99	129.64	146.50	146.39
4	190.06	189.77	201.64	201.30	219.32	218.82
5	238.65	238.44	243.71	243.25	272.09	271.76
	Rectangular plate ($a/b = 2$)					
	$d/b = 0$		$d/b = 0.1$		$d/b = 0.2$	
1	49.34	49.34	48.99	48.87	48.33	48.19
2	128.23	128.24	127.57	127.22	127.20	126.93
3	285.84	285.93	284.47	283.57	284.99	283.22
4	364.56	364.73	362.56	361.22	363.42	361.73
5	443.22	443.33	441.89	440.37	444.90	443.73
	$d/b = 0.3$		$d/b = 0.4$		$d/b = 0.5$	
1	47.90	47.80	48.03	47.94	48.88	48.79
2	128.82	128.63	133.04	132.90	140.33	140.24
3	288.00	287.04	289.43	288.67	288.06	287.37
4	369.50	368.53	378.53	377.84	389.63	389.37
5	450.86	450.52	454.86	454.76	461.38	461.58

worsens with smaller (c/a) and higher mode number. The maximum discrepancy at the fifth mode is seen to be in the neighborhood of 18%. The agreement is slightly better between the frequencies from the two methods for the rhombic plate. The authors believe here that the I-DEAS produces much lower value for the partially loaded edge case because it fails to apply zero slope condition at the two ends of the CFCF edges.

In the next series of calculations, square and rectangular plates with a circular hole at the center, $h/b = 0.01$ and Poisson's ratio $v = 0.30$ are considered. For the rectangular plate the aspect ratio $a/b = 2$ is used in the

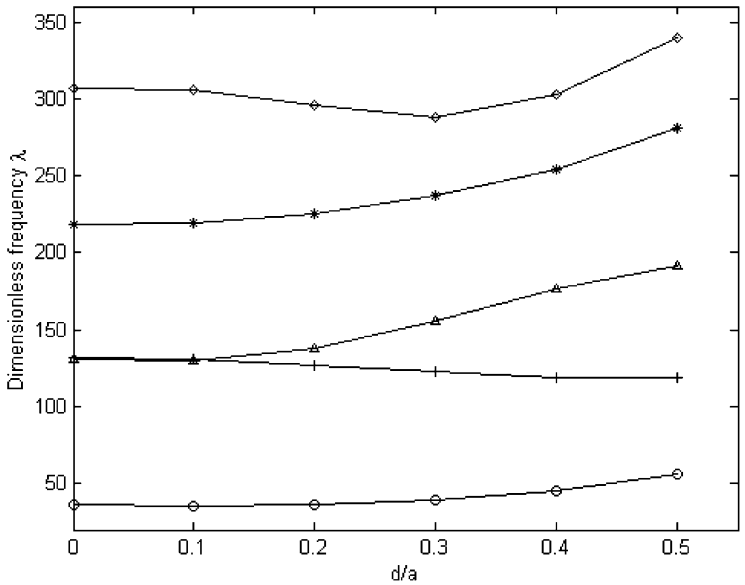

Fig. 12. First five dimensionless frequency values versus the normalized diameter of the hole (d/a) at the center of a square plate with all edges clamped. ○, Mode-1; +, Mode-2; △, Mode-3; ∗, Mode-4; ◇, Mode-5.

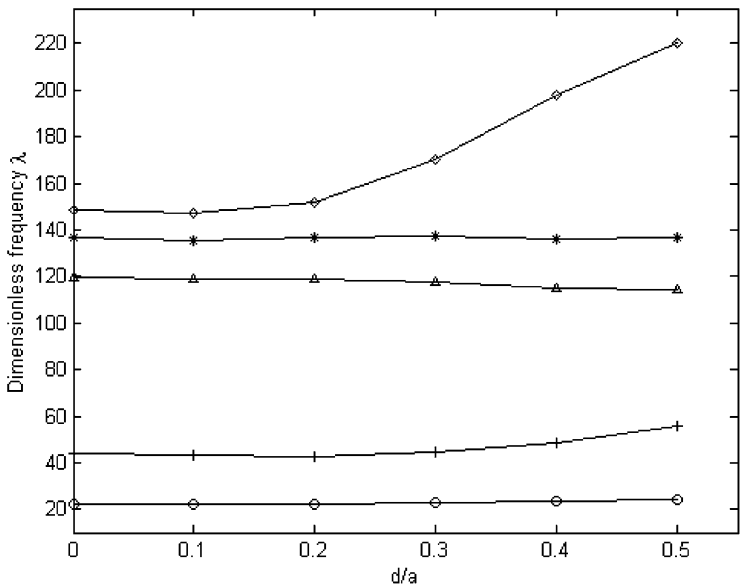

Fig. 13. First five dimensionless frequency values versus the normalized diameter of the hole (d/a) at the center of a square plate with clamped–free–clamped–free edges. ○, Mode-1; +, Mode-2; △, Mode-3; ∗, Mode-4; ◇, Mode-5.

calculation. Results from the present and FE methods are presented in Table 5 for three types of boundary conditions, namely CCCC, CFCF and simply supported–free–simply supported–free (SFSF), respectively. This table also has the results obtained by I-DEAS [25] and very good agreement is found here. To examine the effects of the hole diameters on the dimensionless frequency parameters of square and rectangular plates with $h/b = 0.01$ and Poisson's ratio $v = 0.30$ and all sides SSSS, are calculated and presented in Table 6. Hole-diameters used in the calculation are: $d/b = 0$, 0.1, 0.2, 0.3, 0.4, and 0.5. The two sets of results are in excellent agreement. After comparing results with I-DEAS, the frequency parameters for square plates are calculated for boundary conditions CCCC, CFCF and SFSF and plotted against the normalized diameter of the hole at

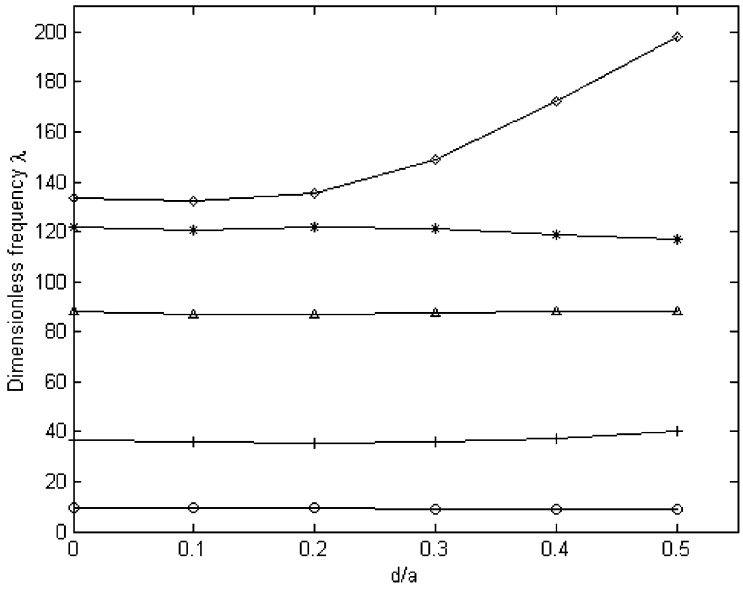

Fig. 14. First five dimensionless frequency values versus the normalized diameter of the hole (d/a) at the center of a square plate with simply supported–free–simply supported–free edges. ○, Mode-1; +, Mode-2; △, Mode-3; ∗, Mode-4; ◇, Mode-5.

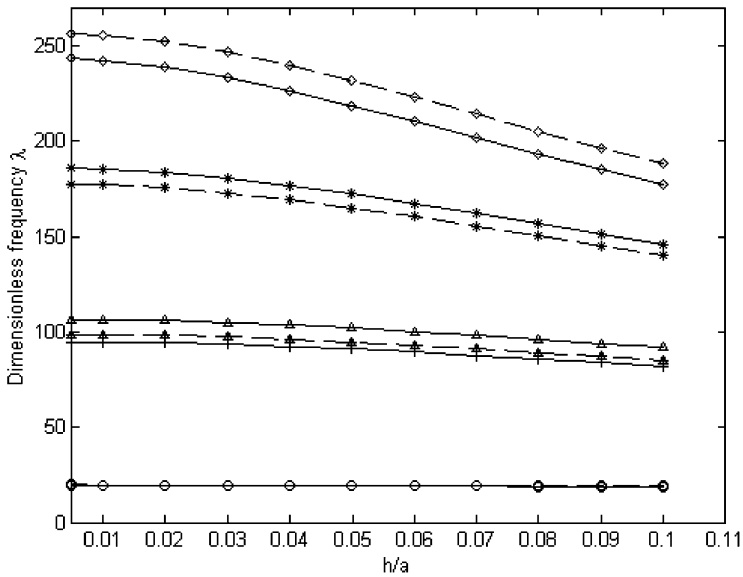

Fig. 15. First five dimensionless frequency values versus the normalized thickness (h/a) for a square plate with a circular hole at the center with edges simply supported. Solid line—$d/a = 0.25$, dashed line—$d/a = 0$; ○, Mode-1; +, Mode-2; △, Mode-3, ∗, Mode-4; ◇, Mode-5.

the center in Figs. 12–14, respectively. The first mode frequencies generally remain unchanged except for the CCCC case for which the frequency parameter increases with the hole-diameter. Other modes show different variation patterns depending upon the boundary conditions.

Figs. 15–18 contain the plots showing the variation of the frequency parameter against the thickness parameter (h/a) for the SSSS boundary condition and the three cases just mentioned above. In these figures, results for the square plates with and without the hole and having $d/a = 0.25$ are plotted by solid and dashed lines, respectively. The values of $\lambda = \omega a^2\sqrt{\rho h/D}$ for the first mode generally remain constant with the varying

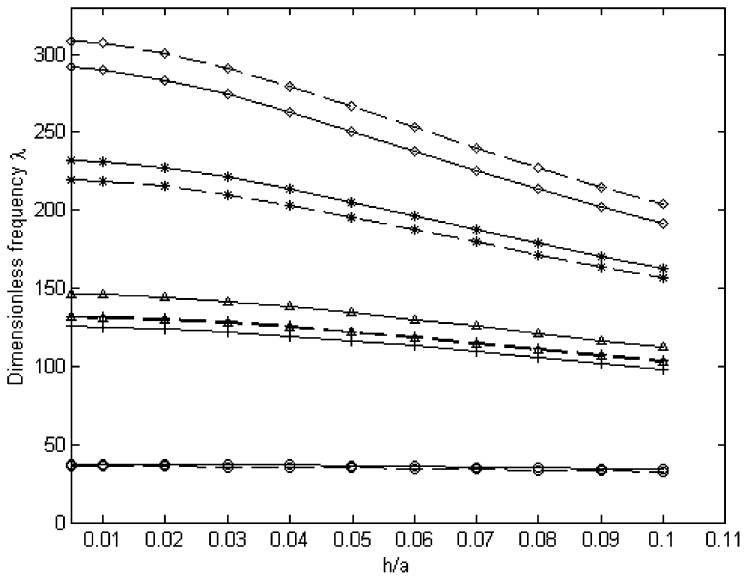

Fig. 16. First five dimensionless frequency values versus the normalized thickness (h/a) for a square plate with a circular hole at the center with all edges clamped. Solid line—$d/a = 0.25$, dashed line—$d/a = 0$; ○, Mode-1; +, Mode-2; △, Mode-3; ∗, Mode-4; ◇, Mode-5.

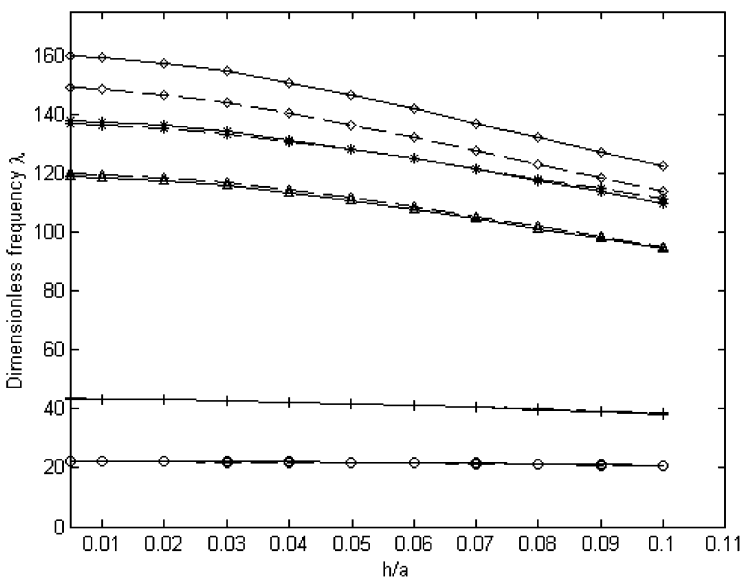

Fig. 17. First five dimensionless frequency values versus the normalized thickness (h/a) for a square plate with a circular hole at the center with clamped–free–clamped–free edges. Solid line—$d/a = 0.25$, dashed line—$d/a = 0$; ○, Mode-1; +, Mode-2; △, Mode-3; ∗, Mode-4; ◇, Mode-5.

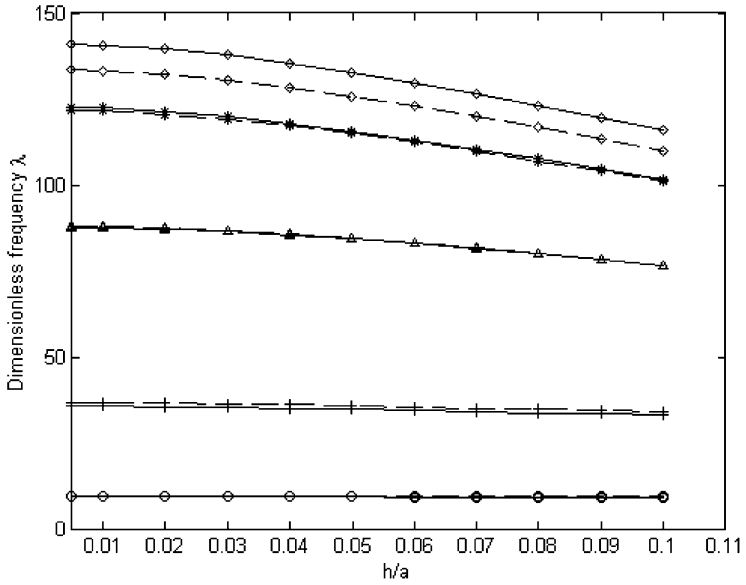

Fig. 18. First five dimensionless frequency values versus the normalized thickness (h/a) for a square plate with a circular hole at the center with simply supported–free–simply supported–free edges. Solid line—$d/a = 0.25$, dashed line—$d/a = 0$; ○, Mode-1; +, Mode-2; △, Mode-3; ∗, Mode-4; ◇, Mode-5.

h/a. In such case the actual frequency increases linearly with the thickness of the plate. For the higher modes of vibration, the frequency parameter λ decreases with h/a. For these cases as well the actual frequency increases with the thickness, but the rate of increase with respect to the plate thickness decreases along the h/a axis. This can possibly be due to the rotary inertia and shear deformation terms included in the formulation. Their effects are quite significant at the higher modes.

6. Concluding remarks

A numerical investigation dealing with buckling and free vibration of doubly connected first-order shear deformable plates has been presented in this paper. Square and rhombic plates are considered as numerical examples for which the results are compared successfully with published data in the literature and also the finite element results. Square and rectangular plates with a circular hole at the center have also been considered in this investigation. It is found that the buckling coefficient decreases with the increasing diameter of the circular opening in the plate. The change in thickness of the plate seems to have very minor effect on the value of the buckling coefficient. Numerical results are also calculated for rhombic plates with large values of the skew angles $\alpha = 60^\circ$ and $\alpha = 75^\circ$. For the case of the vibrating plate, the frequency parameter $\lambda = \omega a^2\sqrt{\rho h/D}$ generally remains constant with the change in the hole-size for the fundamental mode, except for the case when the plate is clamped on all of its four sides. The frequency parameter at the fifth mode of this case decreases initially and then starts increasing for openings with diameter greater than 30% of the length of the plate, i.e. ($d/a > 0.3$). From the successful use of the p-type numerical method in this paper, it is seen that a wide range of plate buckling and vibration problems can be solved accurately.

References

[1] S.P. Timoshenko, J.M. Gere, *Theory of Elastic Stability*, second ed, McGraw-Hill Book Co., New York, 1963.
[2] P.S. Bulson, *The Stability of Flat Plates*, Chatto and Windus, London, GB, 1970.
[3] A.W. Leissa, J.-H. Kang, Exact solutions for vibration and buckling of an SS-C-SS-C rectangular plate loaded by linearly varying in-plane stresses, *International Journal of Mechanical Sciences* 44 (2002) 1925–1945.

[4] J.-H. Kang, A.W. Leissa, Exact solutions for the buckling of rectangular plates having linearly varying in-plane loading on two opposite simply supported edges, *International Journal of Solids and Structures* 42 (2005) 4220–4238.
[5] S.F. Bassily, S.M. Dickinson, Buckling and lateral vibration of rectangular plates subject to in-plane loads—a Ritz approach, *Journal of Sound and Vibration* 22 (2) (1972) 219–239.
[6] S.F. Bassily, S.M. Dickinson, Buckling and vibration of in-plane loaded plates by a unified Ritz approach, *Journal of Sound and Vibration* 59 (1) (1978) 1–14.
[7] S.M. Dickinson, The buckling and frequency of flexural vibration of rectangular isotropic and orthotropic plates using Raleigh's method, *Journal of Sound and Vibration* 61 (1) (1978) 1–8.
[8] T. Mizusawa, T. Kajita, M. Naruoka, Buckling of skew plate structures using B-spline functions, *International Journal of Numerical Methods in Engineering* 15 (1980) 87–96.
[9] T. Mizusawa, T. Kajita, Vibration of skew plates resting on point supports, *Journal of Sound and Vibration* 115 (2) (1987) 243–251.
[10] K.M. Liew, Y. Xiang, S. Kitipornchai, Research on thick plate vibration: a literature survey review, *Journal of Sound and Vibration* 180 (1) (1995) 163–176.
[11] S. Kitipornchai, Y. Xiang, C.M. Wang, K.M. Liew, Buckling of thick skew plates, *International Journal for Numerical Methods in Engineering* 36 (1993) 1299–1310.
[12] K.M. Liew, C.M. Wang, Elastic buckling of regular polygonal plates, *Thin-walled Structures* 21 (1995) 163–173.
[13] K.M. Liew, Y.Q. Huang, J.N. Reddy, Moving least squares differential quadrature method and its application to the analysis of shear deformable plates, *International Journal for Numerical Methods in Engineering* 56 (2003) 2331–2351.
[14] K.M. Liew, J. Wang, T.Y. Ng, M.J. Tan, Free vibration and buckling analyses of shear deformable plates based on FSDT meshfree method, *Journal of Sound and Vibration* 276 (2004) 997–1017.
[15] K.M. Liew, X.L. Chen, J.N. Reddy, Mesh-free radial basis function method for buckling analysis of non-uniformly loaded arbitrarily shaped shear deformable plates, *Composite Methods in Applied Mechanics and Engineering* 193 (2004) 205–224.
[16] K.M. Liew, X.L. Chen, Buckling of rectangular Mindlin plates subjected to partial in-plane edge loads using the radial point interpolation method, *International Journal of Solids and Structures* 41 (2004) 1677–1695.
[17] K.M. Liew, X.L. Chen, Mesh-free radial point interpolation method for the buckling analysis of Mindlin plates subjected to in-plane point loads, *International Journal for Numerical Methods in Engineering* 60 (2004) 1861–1877.
[18] K.M. Liew, Y.Q. Huang, J.N. Reddy, Analysis of general shaped thin plates by the moving least-squares differential quadrature method, *Finite Elements in Analysis and Design* 40 (2004) 1453–1474.
[19] K.M. El-Sawy, A.S. Nazmy, Effect of aspect ratio on the elastic buckling of uniaxially loaded plates with eccentric holes, *Thin-Walled Structures* 39 (2001) 983–998.
[20] M. Huang, T. Sakiyama, Free vibration analysis of rectangular plates with variously shaped holes, *Journal of Sound and Vibration* 226 (4) (1999) 769–786.
[21] A.V. Singh, T. Muhammad, Free in-plane vibration of isotropic non-rectangular plates, *Journal of Sound and Vibration* 273 (2004) 219–231.
[22] T. Muhammad, A.V. Singh, A *P*-type solution for the bending of rectangular, circular, elliptic and skew plates, *International Journal of Solids and Structures* 41 (2004) 3977–3997.
[23] T. Muhammad, A.V. Singh, The buckling of rectangular plates with opening using a polynomial method, *Structural Engineering and Mechanics* 21 (2005) 151–168.
[24] W. Weaver Jr., P.R. Johnston, *Finite Elements for Structural Analysis*, Prentice-Hall Inc., Englewood Cliffs, NJ, 1984.
[25] I-DEAS Master Series™, Structural Dynamics Research Corporation, Milford, OH 45150.